On the supramacromolecular structure of core–shell amphiphilic macromolecules derived from hyperbranched polyethyleneimine

Agustin Picco [a], Martin Kraska [b], Haiko Didzoleit [b], Christian Appel [b], Gustavo Silbestri [c], Omar Azzaroni [a], Bernd Stühn [b], Marcelo Ceolin [a,*]

[a] *Instituto de Investigaciones Fisicoquímicas Teóricas y Aplicadas (INIFTA), Universidad Nacional de La Plata, CONICET, CC 16, Suc. 4, 1900 La Plata, Argentina*
[b] *Institute of Condensed Matter Physics, Technische Universität Darmstadt, Hochschulstraße 8, D-64289 Darmstadt, Germany*
[c] *INQUISUR, Departamento de Química, Universidad Nacional del Sur, Avenida Alem 1253, B8000CPB Bahía Blanca, Argentina*

A B S T R A C T

The supramacromolecular structure of core–shell amphiphilic macromolecules (CAMs) with hyperbranched polyethyleneimine (HPEI) cores and fatty acid chain shells (HPEI-Cn) for different chain lengths was investigated both, in colloidal suspension, solid phase and at the air–water interface using Small Angle X-ray Scattering (SAXS), Wide Angle X-ray Scattering (WAXS), X-ray Reflectometry (XRR) and Langmuir isotherms.

At low temperatures colloidal toluene suspensions of the HPEI-Cn polymers form, as evidenced by peaks arising in the structure factor of the system showing mean particle-to-particle distances correlated with the length of the aliphatic chains forming the shells of HPEI-Cn unimicelles. The CAM sizes as found from the SAXS experiments also display a clear dependence on shell thickness suggesting that the aliphatic chains adopt a brush-like configuration.

After solvent extraction, HPEI-Cn adopts ordered structures with hexagonal packing of the aliphatic chains.

Submitted to lateral pressure Π at the air–water interface, HPEI-Cn undergoes a disorder–order transition with increasing transition pressure for increasing chain lengths. The CAMs show different behaviors in-plane and out-of-plane. While out-of-plane the aliphatic chains behave as a brush remaining almost fully unfolded, whereas parallel to the air–water interface the chains fold down in a mushroom way with increasing lateral pressure Π.

1. Introduction

The search for smart building blocks has attracted the attention of the soft-matter community for a while [1–3]. Among others, amphiphilic building blocks have the ability to adopt several structural conformations by tuning their thermodynamic variables [4].

Along these lines, dendrimers and dendrimeric structures with amphiphilic core–shell architectures displaying micelle-like properties, proved to be attractive building blocks to form supramolecular materials with designed properties [5,6]. Seminal works of Percec [7–9] and Meijer [10], and their co-workers, provided the framework for designing an unprecedented number of superstructural assemblies from precisely engineered dendrons and dendrimers.

In particular, the modification of peripheral groups of hydrophilic dendrimers with hydrophobic tails led to the creation of molecularly defined systems with inverse micelle properties [10,11]. However, dendrimer synthesis is time consuming and limits their application almost to laboratory scale. Alternatively, core–shell amphiphilic macromolecules (CAMs) [12,13] with hyperbranched cores [14], a less perfect variant of the dendrimers have gained popularity, among other properties because of the possibility of easy synthesis of unimolecular micelles [15–17].

CAMs with unimolecular micelar (unimicelar) structures can behave in different ways allowing a tuning of their aggregation state depending on solvent, temperature conditions [18] external fields, pressure, etc. Unimicelles derived from hyperbranched polyethyleneimine (HPEI) are very well known, and they probe their versatility as phase transfer agents among other properties [19–23]. Despite the number of papers reporting results in

* Corresponding author. Address: Instituto de Investigaciones Fisicoquímicas Teóricas y Aplicadas, UNLP-CONICET, Diagonal 113 y 64, 1900 La Plata, Argentina. Fax: +54 221 4254642.
E-mail address: mceolin@inifta.unlp.edu.ar (M. Ceolin).

solution/suspension using HPEI as polar core, to date, there is a lack of information on the structure of HPEI CAMs in solid state.

However, molecular and supramolecular properties are far from being the ultimate hierarchical level and interesting properties arise from supramacromolecular assembly [24]. Recently, we used supramacromolecular assemblies of HPEI-C16 to organize gold nanoparticles into lamellar structures [21]. Among other techniques, Langmuir–Blodgett film assembly has proven to be one of the most versatile methods for controlled assembly of interfacial dendritic structures [25–32].

In this paper we investigate the supramacromolecular structure and properties of the amphiphilic structure (HPEI-Cn) formed by the hyperbranched polar polymer polyethyleneimine (HPEI) and long chain saturated fatty acids (Cn, $n = 8$, 10, 12, 14, 16 and 18. From now on, Cn will indicate the whole set of chain lengths) in toluene suspension, solid state and Langmuir films at air–water interface.

2. Materials and methods

Hyperbranched polyethyleneimine (HPEI, Mn = 10,000 Da) and fatty acid chlorides (capryl, capric, lauryl, myristoyl, palmitoyl and stearoyl chlorides) were purchased from Sigma–Aldrich. Triethylamine (TEA) was purchased from Sintorgan. All chemicals and solvents used were of the maximum purity available in market. Prior to use, HPEI was kept in vacuum for 2 days, chloroform and TEA were purified and dried following standard protocols [33].

The synthesis of HPEI capped with carboxylic acids via amide bound was done according to well established protocols [34,35]. All the compounds were synthesized with a degree of capping of 52% (ratio between acid bound and amines on HPEI). Briefly, HPEI was dissolved in chloroform and TEA was added (1.3/1 M ratio relative to the expected amount of carboxylic acid to be used). The whole system was degassed and filled with Nitrogen or Argon. The corresponding amount of carboxylic acid (1.05/1 M ratio respect of the stoichiometric amount to achieved de desired capping density) was added dropwise and kept at room temperature for 2–3 days under stirring. The opalescent mixture was filtered and the organic phase was washed several times with 2% Na_2CO_3 and NaCl aqueous solutions. The organic phase was dried using Na_2SO_4, and the solvent was evaporated. The solid was kept in vacuum until constant weight (2–3 days).

All the products were characterized by ^1H, ^{13}C NMR and FTIR. NMR spectra were recorded on a Bruker ARX 300 (300.1 MHz for 1H, 75.5 MHz for 13C) using $CDCl_3$ as solvent and $SiMe_4$ as internal reference. Fourier Transformed Infrared spectra were recorded on a Nicolet–Nexus FTIR and a Varian 660 FTIR. The primary-to-secondary-to-tertiary amine ratio of HPEI was checked by 1D-^{13}C-NMR and determined to be 31:41:28 [36] (see supporting information for further details).

Small Angle X-ray Scattering (SAXS) experiments were performed using the SAXS2 station of Laboratorio Nacional de Luz Sincrotron, Campinas, Brazil. The X-ray wavelength was kept to $\lambda = 0.16083$ nm and the sample-to-detector distance was set to 55 cm. All the experiments were performed at constant (22 °C) temperature. Data treatment followed standard procedures to account for beam intensity variations, sample absorption and dark current and background subtraction.

Wide angle X-ray Scattering (WAXS) experiments were performed using a Siemens D500 diffractometer equipped with a conventional X-ray tube operating at a wavelength of $\lambda = 0.15418$ nm (Cu Kα). The X-ray beam was collimated by two slits before hitting the sample. A monochromator crystal was placed in front of the detector (scintillation counter). The resulting diffraction pattern has been corrected for sample cell scattering.

For monolayer experiments a modified Langmuir trough system (maximum area: 220 cm^2, Kibron Inc., Finland) has been used. For in situ X-ray reflectivity (XRR) of the HPEI-Cn monolayers the trough system is placed on an active vibration isolation system (HWL Scientific, TS150) included in a X-ray reflectometer (D8 Advance, Bruker AXS) also using Cu Kα radiation. Here, the beam is collimated by two slits and monochromized by a Goebel mirror (W/Si multilayer mirror). The intensity is detected by a Vântec-1 line detector (Bruker AXS). Reflectivities were analyzed as described elsewhere [37,38]. The Langmuir monolayers were prepared as follows: suspensions of HPEI-Cn in chloroform (Sigma Aldrich, +99%) were prepared at concentrations of 1 mg/ml. A constant volume of 20 µl was subsequently spread onto the clean water surface with a 10 µl Eppendorf pipette. We waited approximately 15 min to let the chloroform evaporate before compressing with a constant velocity of 1 cm^2/min. Resulting compression isotherms are given as function of the surface mass concentration Γ of HPEI-Cn. The surface tension γ of the liquid/air interface is measured with a Wilhelmy needle and compared to the surface tension γ_0 of the bare water surface to yield the surface pressure $\Pi = \gamma_0 - \gamma$.

3. Results and discussion

3.1. HPEI-Cn CAMs suspended in toluene

The amphiphilic nature of HPEI-Cn with a hydrophilic core partially shielded by an aliphatic shell (the degree of capping in our CAMs was kept fixed at 52%) opens the possibility to tune the supramacromolecular structure of the micelles controlling solvent properties (temperature, electric susceptibility, etc.). In fact, Picco et al. [18] showed that HPEI-C16 displays a liquid crystal-to-colloid thermally activated transition near room temperature. Moreover, HPEI-C16 displays also negative thermal expansion of the interplanar distance below the transition temperature suggesting a complex interplay between energetic contributions (Van der Waals interactions between aliphatic chains, hydrophobic core-solvent interactions) and entropic contributions due to organized solvent around shell chains.

Fig. 1A shows the SAXS data obtained from HPEI-Cn ($n = 8$, 10, 12, 14, 16 and 18) suspended at 10 g/l in toluene at 5 °C. The choice of the sample concentration was dictated by a compromise between reasonable signal-to-noise ration in the SAXS experiments and long enough (more than 30 min) colloidal stability of the samples. Depending on chain length, two main features can be observed in the diagrams: (i) between 1.5 nm^{-1} ($d = 4.2$ nm) and 3.0 nm^{-1} ($d = 2.1$ nm) a clear broad structure maximum can be observed (very clear for $n = 14$, 16 and 18). Above 3.0 nm^{-1}, HPEI-C14 to –C18 also display a minimum attributable to the form factor $P(q)$ of the scatters (HPEI-Cn) forming the structure observable at lower q.

Assuming that the scatters are spherical particles (a simplified assumption), the position of the minimum in the form factor relates to the radius of the sphere as $q_{min}R = 4.48$. Using this expression, the radii of the individual HPEI-Cn ($n = 14$, 16 and 18) follow a straight line (Fig. 1B) with a slope $m = 0.125 \pm 0.003$ nm/atom in good agreement with the length increment expected for the alkyl chains of the shell [39]. However, the ordinate obtained from the fit $b = -0.67 \pm 0.05$ nm has an unphysical negative value although it should represent the (positive!) radius of the bare HPEI nucleus. While the linear model seems to be correct for $n > 14$, deviations should be expected for shorter aliphatic chains in order to circumvent the problem.

The broad features observed in the SAXS diagrams between 1.5 and 3 nm^{-1} can be attributed to the structure factor originated in the interaction between individual HPEI-Cn CAMs. A remarkable
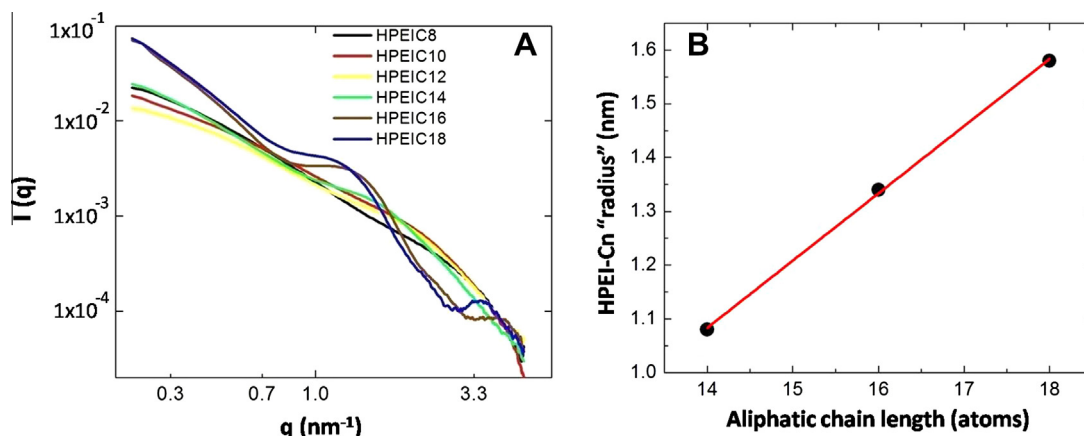
Fig. 1. SAXS diagrams (A) obtained for toluene suspensions (10 g/l) of HPEI-Cn. HPEI-Cn size (B) obtained from the minimum observed around $q = 3$ nm^{-1} in panel A. See main text for details.SAXS diagrams (A) obtained for toluene suspensions (10 g/l) of HPEI-Cn (C8: black, C10: red, C12: yellow, C14: green, C16: brown and C18: blue). HPEI-Cn size (B) obtained from the minimum observed around $q = 3$ nm^{-1} in panel A. See main text for details.

fact is that the per-carbon-atom increment of the distance associated with the structure factor is 0.33 nm/atom (more than twice the value obtained from the form factor) suggesting that the structure formed from the interaction between CAMs has a dynamic character and cannot be associated with permanent aggregates.

3.2. HPEI-Cn CAMs deposited on flat substrates

Fig. 2A displays the SAXS diagrams obtained for HPEI-Cn ($n = 12$, 14, 16 and 18) at 20 °C as dry powders after solvent (chloroform) extraction. All SAXS diagrams display clear peaks
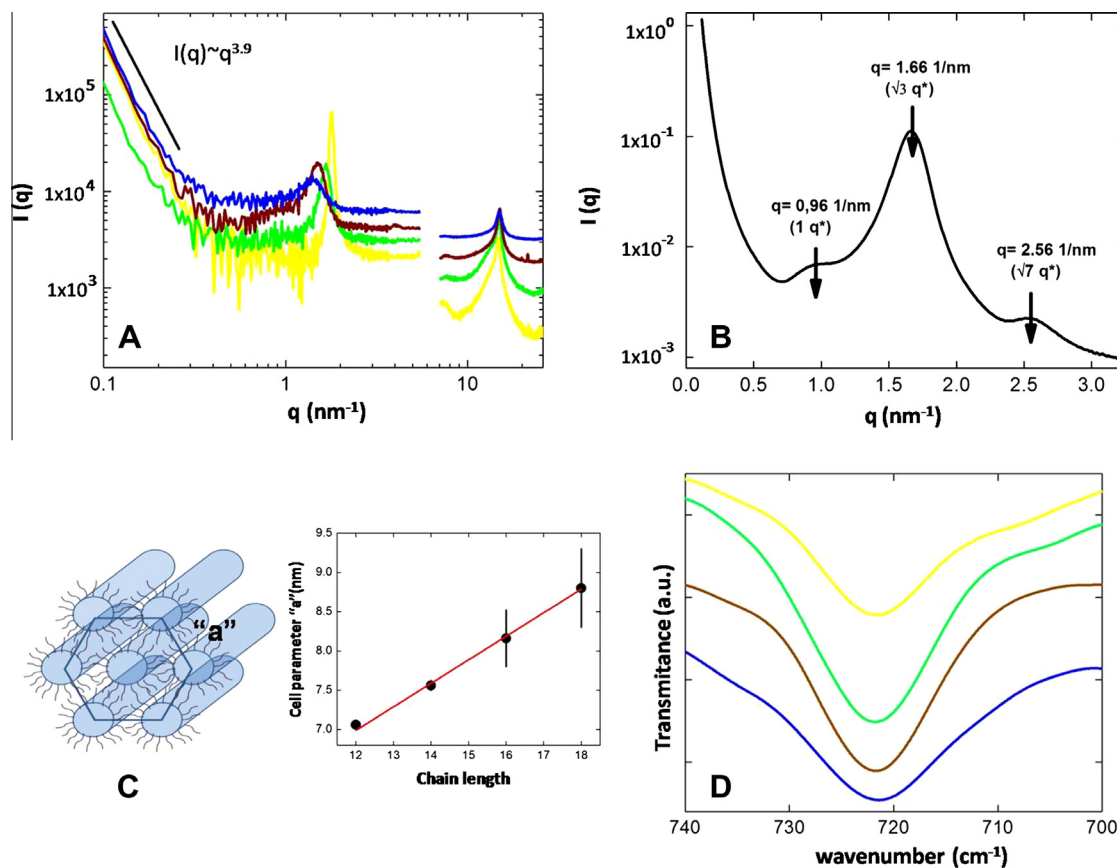

Fig. 2. SAXS and Infra-red data obtained from dried HPEI-Cn ($n = 12$, 14, 16 and 18) samples. (A) Full scattering curves. Left: SAXS region. Right: WAXS region. The curves were vertically shifted for clarity. (B) SAXS curve obtained for HPEI-C14 showing the position of the diffraction peaks (C) Schematic view (left) of the 2D-hexagonal structure deduced for dried HPEI-Cn and linear correlation (right) between the cell parameter "a" of the hexagonal structure and the aliphatic chain length "n". The red line corresponds to the fitted curve. (D) FTIR spectra showing the region corresponding to the rocking modes of the aliphatic Cn chains. HPEI-C12 (yellow), HPEI-C14 (green), HPEI-C16 (brown) and HPEI-C18 (blue). See main text for details.

indicating that dry HPEI-Cn powders form "long range" ordered structures. Detailed analysis of the SAXS data indicate the existence of various diffraction peaks escorting the main feature around 1.7–1.8 nm^{-1}.

Fig. 2B shows a detailed analysis of the diagram obtained for HPEI-C14 (also shown in Fig. 2A). Three Bragg peaks at q^*, $(\sqrt{3})q^*$ and $(\sqrt{7})q^*$ can be observed indicating that HPEI-C14 forms ordered 2D-hexagonal phases (the Bragg peak with $q = 2q^*$ is hidden within the intense $\sqrt{3}$ peak). Although several authors have observed columnar hexagonal phases in similar systems [40], a brief comment must be introduced indicating that other possible structures can be suggested without essential changes in our further reasoning. Hence, several authors reported other structures compatible with our SAXS results as lamellae (in fact the intensity of the second Bragg peak suggests a possible coexistence with a lamellae phase or even intermediate phases between lamellar and columnar structures), deformed hexagonal structure [41], perforated hexagonal phases and rippled lamellar structures [42].

A similar 2D-hexagonal structure can be deduced for HPEI-C12, HPEI-C16 and HPEI-C18 displaying $\sqrt{1}q^*$, $\sqrt{3}q^*$ and $\sqrt{7}q^*$ characteristic peaks.

Assuming columnar hexagonal arrangement, the peak $q(hkl)$ position for 2D-hexagonal structures can be written in terms of the cell parameter "a" as:

$$\frac{2\pi}{d(hk0)} = q(hk0) = 4\pi\sqrt{\frac{h^2 + hk + k^2}{3a^2}} \qquad (1)$$

Thus, the position of the first two peaks relates to the lattice parameter "a" as $q(100) = 4\Pi/a\sqrt{3}$ and $q(110) = 4\Pi/a$, being "a" the transversal hexagonal lattice parameter and the distance between the centers of cylinders (see Fig. 2C, left).

Eq. (1) allows obtaining the cell parameter "a" from the position of Bragg peaks observed for HPEI-Cn. The arithmetic average for "a" (taken over the peaks $(hkl) = (100)$, (110) and (210)) obtained for every aliphatic chain length can be seen in Table 1 and are plotted in the right panel of Fig. 2C. A linear fit ($a = D_0 + m * N_{carbon}$ as suggested by Thünemann [43]) to the experimental data yields an ordinate $D_0 = 3.55 \pm 0.39$ nm and a slope $m = 0.29 \pm 0.03$ nm/carbon atom. Here, D_0 should corresponds to the diameter of the bare HPEI core under the conditions imposed by the solid packing and m represents twice the contribution of each carbon atom to the length of the aliphatic chain. Recently, Tsiourvas and Arkas [44] reported the observance of columnar phases displaying ellipsoidal cores formed by 5 kDa HPEI (PDI = 1.3) in fully alkylated HPEI-Cn derived CAMs, in coincidence with our results.

As expected, the slope m obtained from the linear fit coincides fairly well with twice the expected C–C bond length for aliphatic chains (~0.28 nm) due to the presence of two extending chains covering the space in between the HPEI cores.

Tanford [39] proposed that the length of an extended aliphatic chain can be correlated with its carbon number as $L_c = (0.15 + 0.1265\, N_{carbon})$nm. The values obtained from the latter formula for $N_{carbon} = 12, 14, 16$ and 18 can be found in Table 1. Although somewhat higher, our values for the chain length

coincide rather well with those obtained from Tanford's formula, indicating that the aliphatic chains remain fully unfolded in a "brush-like" configuration.

The lateral packing of the aliphatic chains in the shell can be addressed using WAXS and FTIR. There are a few common ways of packing aliphatic chains: orthorhombic (βo), Triclinic (βt) (and also Monoclinic) and hexagonal (αh) differing on their WAXS and FTIR signals [45,46].

From WAXS experiments it is possible to distinguish three different crystal structures having the following average characteristic position for their main diffraction peaks (reciprocal space between parenthesis): hexagonal (αh): 0.42 nm (15 nm^{-1}), orthorhombic (βo): 0.42 nm (15 nm^{-1}) and 0.38 nm (16.5 nm^{-1}), triclinic (βt): 0.45 nm (14 nm^{-1}), 0.38 nm (16.5 nm^{-1}) and 0.36 nm (17.5 nm^{-1}).

Fig. 2A includes the WAXS diagrams of the HPEI-Cn compounds. In all cases, a diffraction peak in the range of 14.7–15.0 nm^{-1} is observed indicating mean interplanar distances around 0.42 nm almost independent of the chain length, typical for hexagonal (αh).

There are several examples of this kind of analysis for polymer-surfactant complexes [47–51] supporting the assignment.

Supporting the WAXS results, FTIR can also provide useful information on the packing structure of aliphatic chains analyzing the 720 cm^{-1} region of the spectrum. This region, corresponds to the rocking modes of the aliphatic chains, and is observable for chains longer than 4 carbons in linear configuration. For the orthorhombic packing (βo), the rocking modes display two bands located at 719 cm^{-1} and 727 cm^{-1}. Hexagonal and triclinic packing shows a single band, located around 717 cm^{-1} (for triclinic, βt) and 720–721 cm^{-1} (for hexagonal, αh) [48,52]. Examples of the use of the rocking mode to analyze the lateral packing of aliphatic chains in polymeric complex can be found in the works of Luyten [48] and Ren [53].

Our FTIR spectra (Fig. 2D), reveal in all cases a single rocking band centered at 721 cm^{-1} reinforcing the conclusion that the lateral packing of the aliphatic shell chains should be hexagonal (αh).

These results are in fairly good agreement with those reported by Mezzenga and co-workers for Hyperbranched Poly-Lysine capped with saturated fatty acids [51] and Lee et al. for isocyanate capped hydroxypropylcellulose [50].

As a last point, SAXS data at low q (Fig. 2A, below 0.5 nm^{-1}) scale as q^{-m} ($m \approx -3.9$) for every chain length indicate that the ordered domains have rather 3D structure with smooth surfaces.

3.3. HPEI-Cn CAM's at the air–water interface

Up to now we have shown that HPEI-Cn form aggregates in toluene suspensions and those dynamic structures form well defined
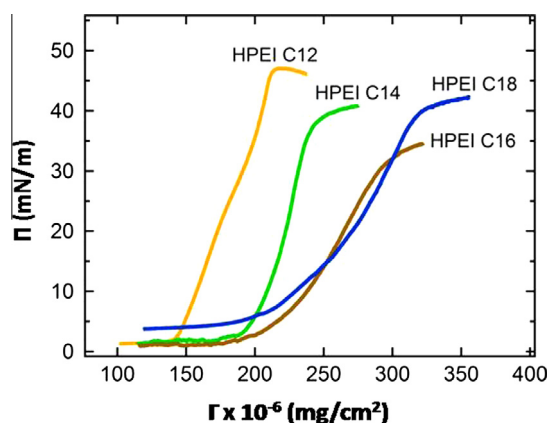
Table 1
Center-to-center distance as obtained from the SAXS data of HPEI-Cn for different chain lengths assuming hexagonal arrangement. The values are the arithmetic average of the individual obtained for $(hkl) = (100)$, (110) and (210). The error quoted is the standard deviation of the mean.

Compound	a (nm)	L_c (nm) exp.	L_c (nm) Tanford
HPEI-C12	7.06 ± 0.06	1.76	1.68
HPEI-C14	7.56 ± 0.06	2.05	1.91
HPEI-C16	8.16 ± 0.36	2.30	2.17
HPEI-C18	8.80 ± 0.50	2.63	2.42

Fig. 3. Compression isotherms of HPEI-Cn molecules on water.

long-range structures after solvent removal. Now we are interested in investigating the order and structure of Langmuir monolayers of HPEI-Cn assembled on top of the air–water interface of a Langmuir–Blodgett trough. Fig. 3 shows the compression isotherms of the HPEI-Cn molecules. In all cases well defined monolayers could be obtained indicating a surface activity though the fraction of hydrophilic groups within the particles is small. At low surface concentrations Γ of HPEI-Cn a nearly zero surface pressure Π indicates a dilute situation where the molecules barely interact forming a "gas phase". At the concentration Γ^{crit} the molecules begin to overlap (this concentration is defined as the point where the first pronounced increase of Π appears). The following steep increase in Π ends at a critical surface pressure Π_c where the monolayer either collapses or molecules dissolve in water. The qualitative compression behavior of the monolayers roughly equals each other but a strong shift of the isotherms is observed depending on the type of fatty acid attached to the HPEI molecule. Remembering that the degree of capping for the particles is 52% therefore we expect the fatty acids at least to be in a more or less stretched brush like state. From the overlap concentration Γ^{crit} we calculated effective radii R_{eff} assuming that the area needed by one molecule is given by a circular area. The results are shown in Fig. 4A as a function of the number of carbon atoms of the attached fatty acids onto the HPEI molecule. Similar to the intermicellar distance in dried phase (see above), R_{eff} follows a linear relation

$$R_{eff}(n) = (0.04 \pm 0.01)\text{nm} \cdot n + (2.75 \pm 0.11)\text{nm} \qquad (2)$$

giving a radial increase of 0.04 nm per added carbon atom. This value is a factor of 3 smaller than the carbon–carbon distance indicating a rather soft character of the "in-plane" fatty acid shell of the HPEI-Cn. The ordinate represents the extrapolation of R_{eff} on the water surface, to zero carbon atoms attached, namely the bare molecule, of R_{eff} on the water surface. The value of 2.75 nm gives a diameter of 5.5 nm, slightly larger than the diameter obtained in bulk (see above). This result might not be surprising and may be due to a more flat conformation on top of the water surface. This assumption is supported by our in situ XRR results which will be discussed later.

A closer look on the compression isotherm of the smallest molecule – HPEI-C12 – we observe two distinct regions in the steep increase of Π expressed by a change in the slope of Π. We extrapolated both regimes to $\Pi = 0$ and obtain two different values for R_{eff} (see Fig. 4A). This might be due to a structural rearrangement on the surface. Another possibility is that the compression is given by two steps. First the fatty acids are compressed followed by a compression/rearrangement of the HPEI core. The slope of the increase in Π can be utilized to gain quantitative information about the compression process. The isothermal compressibility C_s calculated from the compression isotherms by [54]

$$C_s = -\Gamma \cdot \left(\frac{\partial(1/\Gamma)}{\partial\Pi}\right) \qquad (3)$$

is shown in Fig. 5 for every chain length. In the figure the two step compression is clearly seen as two different compressibility regimes ($\sim190 \times 10^6$ and 240×10^6 mg/cm² for HPEI-C12) located at the two minima in C_s. Increasing the number of carbon atoms in the attached fatty acids lead to smearing of the first minimum in C_s at low surface concentration Γ although the two compression steps are still present for all samples. The C_s value obtained from the first minimum corresponds roughly to compressibility values for fatty acids (e.g. 7 m/N for behenic acid [55]). In general we find that for longer fatty acids the overall molecule becomes softer as seen by the global compressibility minimum of the respective sample. This is not surprising because of the increasing relevance of the entropy part of the free energy for longer chains.

To obtain information on the out-of-plane structure of the monolayers, X-ray Reflectivity experiments (XRR) were performed in-situ at selected pressures. A representative set of in-situ reflectivity experiments on HPEI-Cn monolayers is shown in Fig. 6 either for approximately constant pressure and different molecules (Fig. 6A) or for one molecule (HPEI-C12) for different pressures (Fig. 6B). In all cases clear interferences (so called "Kiessig fringes") are visible arising from the interference of the X-rays scattered from the top and the bottom of the monolayer whose position is related to the respective layer thickness d.

It is remarkable that the increase of 6 carbon atoms in the fatty acids leads to a pronounced shift of the interference minimum (see Fig. 6A). Increasing Π (Fig. 6B) the thickness of the monolayer slightly increases possibly due to rearrangement of the fatty acid shell when compressing the HPEI core in the second compression regime.

In order to obtain quantitative information from the reflectivity data, the bare water surface before every monolayer experiment has been analyzed in terms of Fresnel reflectivity [56]

$$R_{water} = (q_z)R_F e^{(-q_z^2\sigma^2)} \qquad (4)$$

with R_F being the Fresnel reflectivity and σ the roughness of the water surface due to thermal capillary wave excitations (typical values found in our experiments are $\sigma = (0.30 \pm 0.01)$ nm as expected for capillary waves at 20 °C [57]). The monolayer reflectivity has been analyzed using IGOR Pro and Motofit [58] which applies a genetic fit algorithm combined with the matrix method [59] to calculate the reflectivity of a layered structure.
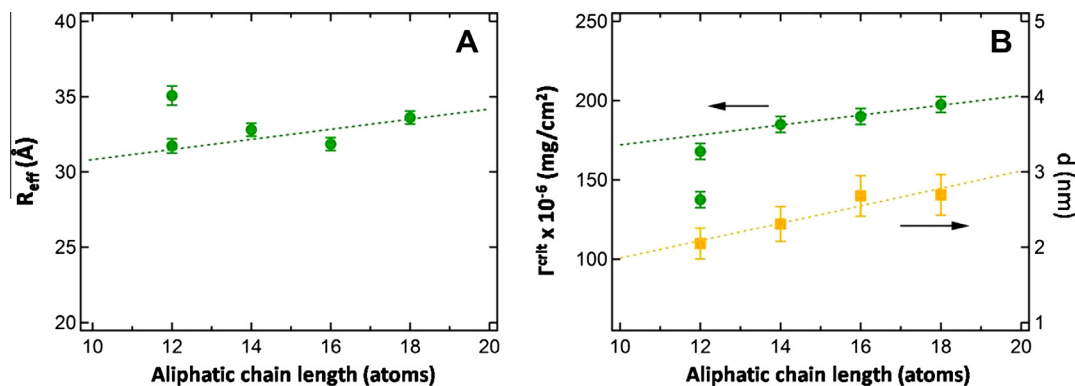

Fig. 4. (a) Effective radii R_{eff} of the HPEI-Cn molecules on the water surface. (b) Overlap concentrations Γ^{crit} (green) and total layer thicknesses measured by XRR of the HPEI-Cn monolayers (yellow).
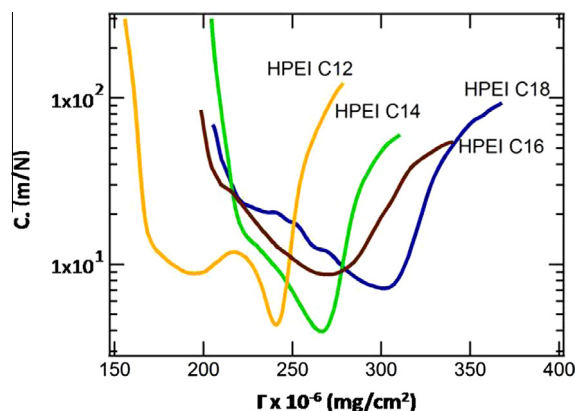
Fig. 5. Isothermal compressibility of HPEI-Cn molecules on the water surface.

Solid lines in Fig. 6 are fits to the data according to a two layer model which consists of a lateral averaged (along the water surface) electron scattering length density (SLD) of the HPEI cores and a second layer of fatty acids on top of the HPEI cores.

When compressing a monolayer of HPEI-Cn we found that the thickness of the HPEI core layer and the fatty acid layer remain almost constant (in a first approximation). We think this is due to a more or less solid like behavior where the whole molecule behaves as a rather hard object on the water surface. Nevertheless,

a slight increase in total layer thickness can be seen in Fig. 7A, possibly due to the "brushing" of the aliphatic shell upon compression.

An interesting effect is that the lateral averaged SLD increases slightly with increasing pressure (data not shown) indicating a decrease of average particle distance on the water surface.

The total thickness of the monolayers for $\Pi = 10 \text{mN/m}$ are shown in Fig. 4B as a function of the number of carbon atoms in the fatty acids. A linear relation is found which follows

$$d(n) = (0.16 \pm 0.03)\text{nm} \cdot n + (0.69 \pm 0.38)\text{nm} \qquad (5)$$

Resulting in a total thickness per added carbon atom to the fatty acids increases by 0.16 nm which means a radial increase of 0.08 nm (see R_{eff} values in Fig. 4A) perpendicular to the water surface.

The ordinate of this linear relation gives the approximation to the thickness of the HPEI core without fatty acids on the water surface. A value ~0.7 nm is rather small and gives a hint for a more flat conformation of HPEI-Cn molecules on the surface as already deduced.

Summing up to results presented above, the fatty acid chains of the shell has two quantitatively different behaviors (i) in-plane, the fatty acid chains behave rather soft as indicated by the small per-carbon-atom increment (0.03 nm) of the center-to-center distance (ii) out-of-plane, the per-carbon-atom increment (0.08) although smaller than the expected for extended aliphatic chains (0.12 nm), is closer to this value indicating a stiffer aliphatic shell.
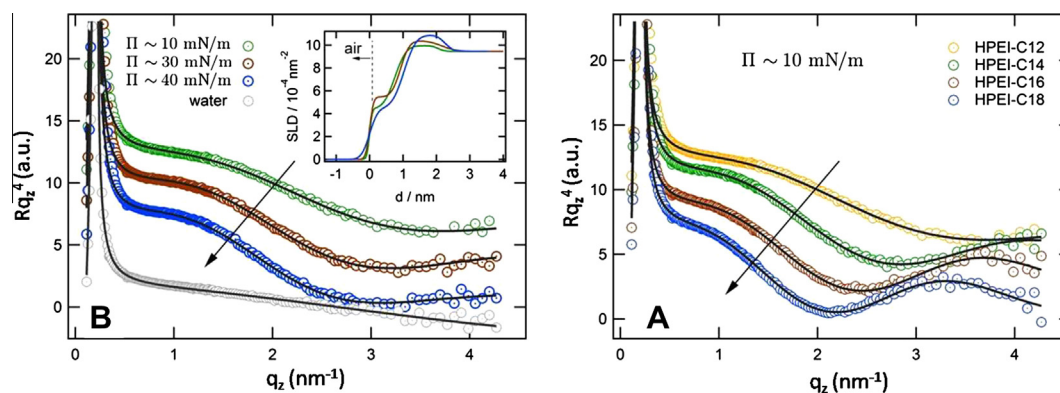

Fig. 6. (A) In situ reflectivity of all HPEI-Cn monolayers at about $\Pi \sim 10$ mN/m. The arrow marks the direction of increasing number of carbon atoms in the attached fatty acids. (B) In situ reflectivity of HPEI-C12 for different Π values. The arrow indicates the direction of increasing Π. Also, the reflectivity for the bare water surface is shown (bottom curve). All reflectivity are given in arbitrary units and shifted for clarity. Lines are fits to the data according to the two-layer model described in the text for the monolayer systems and according to Eq. (2) for the water surface. Inset: typical electron scattering length density distributions perpendicular to the surface.
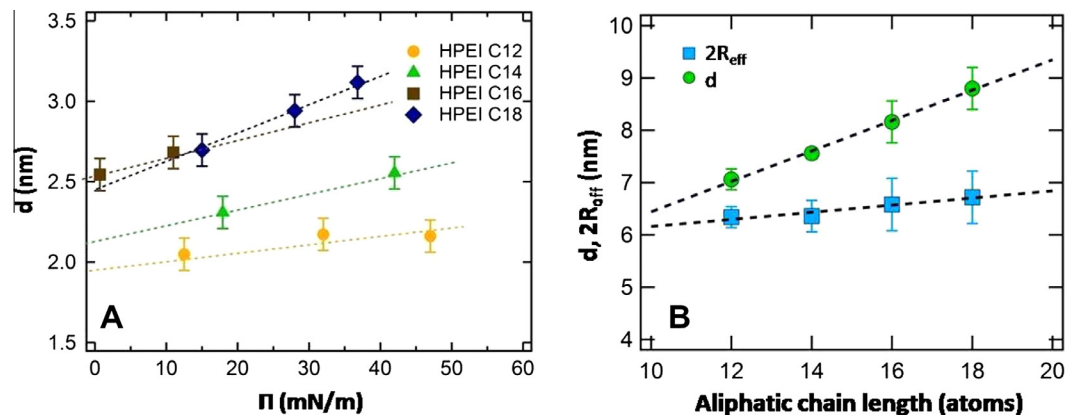

Fig. 7. (A) Total monolayer thickness of HPEI-Cn samples for different surface pressures measured by XRR. The dotted lines are guide for the eyes only. (B) Comparison of the bulk close packing distance of the CAMs and 2 R_{eff} of them on the water surface.
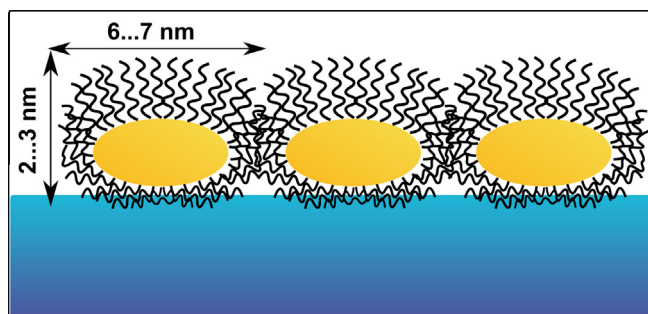
Fig. 8. Proposed conformational arrangement of the HPEI-Cn molecules at the water/air interface.

Combining the size estimations from XRR and Langmuir experiments the dimensions of the particle can be concluded to be more or less flattened or ellipsoid like with an estimated volume of $V \approx 4/3\pi(2.75)^2 \cdot (0.69/2) \approx 11 \text{ nm}^3$. In the bulk powder the volume is comparable to the water surface value. However, the absolute values of the lateral 2 R_{eff} at the water surface and the close packing distance L found in the bulk investigations favorable coincide. Only the slope, meaning the increase of size by increasing number of carbon atoms in the fatty acid moieties, is different possibly due to partially dissolving and deformation of the HPEI core.

To summarize the structural analysis of the HPEI-Cn monolayers we propose the molecular structure to have a more flattened conformation with fatty acid chains in a more brush-like conformation perpendicular to the water surface, and a softer (mushroom-like) lateral conformation where fatty acid chains are barely stretched, see Fig. 8.

4. Conclusions

Supramacromolecular assembly of functional soft-matter structures proves to be a flexible strategy for controlling material properties [1–3] and designing novel collective behavior.

CAMs with hyperbranched polyethyleneimine core building blocks are especially useful acting as unimicelles, based on the ability to transfer polar substances to non-polar media due to the hydrophilic nature of the cores. Previous results on HPEI-C16 unimicelles demonstrated that tight control over thermodynamic variables leads to the formation of supramacromolecular assemblies [18] as well as nanoparticle encapsulation [21].

In this paper we demonstrated that HPEI-Cn assemblies form columnar hexagonal structures after solvent evaporation displaying also hexagonal lateral packing for the aliphatic chains.

We also determined that HPEI-Cn CAMs form unimolecular layers at the air–water interface under controlled lateral pressure in Langmuir–Blodgett experiments. A strong influence of the interface has also been determined forcing the structure of the HPEI-Cn assemblies to be flattened exhibiting a different folding behavior of their aliphatic chains in-plane (mushroom-like) and out-of-plane (brush-like).

Altogether, our results demonstrate the versatility of CAMs as functional bricks for hierarchical assembly and highlight the importance of the strict control of thermodynamic variables during soft-matter supramolecular self-assembly.

Author contributions

The manuscript was written through contributions of all authors. All authors have given approval to the final version of the manuscript.

Appendix A. Supplementary material

Supplementary data associated with this article can be found, in the online version, at http://dx.doi.org/10.1016/j.jcis.2014.06.034.

References

[1] S.I. Stupp, V. LeBonheur, K. Walker, L.S. Li, K.E. Huggins, M. Keser, A. Amstutz, Science 276 (1997) 384–389.
[2] J.M. Lehn, Science 295 (5564) (2002) 2400–2403.
[3] O. Ikkala, G. Ten Brinke, Chem. Commun. 10 (19) (2004) 2131–2137.
[4] S. Dai, P. Ravi, K.C. Tam, Soft Matter 5 (2009) 2513–2533.
[5] D.A. Tomalia, Progress Polym. Sci. 30 (2005) 294–324.
[6] S.M. Grayson, J.M.J. Frechet, Chem. Rev. 101 (2001) 3819–3867.
[7] B.M. Rosen, C.J. Wilson, D.A. Wilson, M. Peterca, M.R. Imam, V. Percec, Chem. Rev. 109 (11) (2009) 6275–6540.
[8] X. Zeng, G. Ungar, Y. Liu, V. Percec, A.E. Dulcey, J.K. Hobbs, Nature 428 (6979) (2004) 157–160.
[9] S.D. Hudson, H.T. Jung, V. Percec, W.D. Cho, G. Johansson, G. Ungar, V.S.K. Balagurusamy, Science 278 (5337) (1997) 449–452.
[10] A.P.H.J. Schenning, C. Elissen-Roman, J.W. Weener, M.W.P.L. Baars, S.J. van der Gaast, E.W. Meijer, J. Am. Chem. Soc. 120 (1998) 8199–8208.
[11] V. Chechik, M. Zhao, R.M. Crooks, J. Am. Chem. Soc. 121 (1999) 4910–4911.
[12] D. Wan, J. Yuan, H. Pu, Macromolecules 42 (2009) 1533–1540.
[13] D. Wan, H. Pu, M. Jin, H. Pan, Z. Chang, React. Funct. Polym. 70 (2010) 916–922.
[14] D. Yan, C. Gao, H. Frey, Hyperbranched Polymers: Synthesis, Properties, and Applications, John Wiley and Sons, Hoboken, 2011.
[15] M.C. Jones, J.C. Leroux, Soft Matter 6 (2010) 5850–5859.
[16] T. Satoh, Soft Matter 5 (2009) 1972–1982.
[17] B.I. Voit, A. Lederer, Chem. Rev. 109 (11) (2009) 5924–5973.
[18] A.S. Picco, B. Yameen, O. Azzaroni, M. Ceolin, Chem. Commun. 47 (2011) 3802–3804.
[19] Q. Tang, F. Cheng, X.L. Lou, H.J. Liu, Y. Chen, J. Colloid Interface Sci. 337 (2009) 485–491.
[20] S. Srivastava, D.L. Frankamp, V.M. Rotello, Chem. Mater. 17 (3) (2005) 487–490.
[21] A.S. Picco, E. Zelaya, O. Azzaroni, M. Ceolin, J. Colloid Interface Sci. 397 (2013) 206–209.
[22] Q. Tang, F. Cheng, X.L. Lou, H.J. Liu, Y. Chen, J. Colloid Interface Sci. 337 (2) (2009) 485–491.
[23] S. Stevelmans, J.C.M. Van Hest, J.F.G.A. Jansen, D.A.F.J. Van Boxtel, De Brabander-van Den Berg, E.W Meijer, J. Am. Chem. Soc. 118 (31) (1996) 7398–7399.
[24] R. Backov, Soft Matter 2 (6) (2006) 452–464.
[25] G. Sui, M. Mabrouki, Y. Ma, M. Micic, R.M. Leblanc, J. Colloid Interface Sci. 250 (2) (2002) 364–370.
[26] Z. Jia, M.P. Srinivasan, Colloids Surf. A: Physicochem. Eng. Aspects 257–258 (2005) 183–190.
[27] D.K. Yoon, H.T. Jung, Langmuir 19 (2003) 1154–1158.
[28] E. Wolert, S.M. Setz, R.S. Underhill, R.S. Duran, M. Schappacher, A. Deffieux, M. Haderle, R. Malhaupt, Langmuir 17 (18) (2001) 5671–5677.
[29] S. Reuter, A.M. Hofmann, K. Busse, H. Frey, J. Kressler, Langmuir 27 (5) (2011) 1978–1989.
[30] S. Peleshanko, V.V. Tsukruk, J. Polym. Sci., Part B: Polym. Phys. 50 (2) (2012) 83–100.
[31] D.D. Lu, L.Q. Yang, X.L. Shi, Y. Chang, H. Zhang, Z.Q. Lei, Int. J. Polym. Mater. Polym. Biomater. 61 (5) (2012) 384–394.
[32] J. Paczesny, J. Gregorowicz, K. Nikiforov, Polymer (United Kingdom) 54 (1) (2013) 174–187.
[33] W. Amarego, C. Chai, Purification of Laboratory Chemicals, seventh ed., Elsevier, 2012.
[34] M. Kramer, M. Kopaczynska, S. Krause, R. Haag, J. Polym. Sci., Part A: Polym. Chem. 45 (2007) 2287–2303.
[35] S. Stevelmans, J.C.M. Van Hest, J.F.G.A. Jansen, D.A.F.J. Van Boxtel, E.M.M. De Brabander-van Den Berg, E.W. Meijer, J. Am. Chem. Soc. 118 (1996) 7398–7399.
[36] H. Liu, Z. Shen, Y. Chen, W. Zhang, L. Wei, J. Polym. Sci., Part A: Polym. Chem. 44 (2006) 4165–4173.

[37] M. Kraska, M. Gallei, B. Stühn, M. Rehahn, Langmuir 29 (26) (2013) 8284–8291.
[38] M. Kraska, M. Domchke, B. Stühn, Soft Matter 9 (2013) 3488–3496.
[39] C. Tanford, J. Phys. Chem. 76 (21) (1972) 3020–3024.
[40] K. Lorenz, H. Frey, B. Stühn, R. Mulhaupt, Perfluoroalkyl End Groups, Macromolecules 30 (1997) 6860–6868.
[41] S. Bondzic, E. Polushkin, J. Ruokolainen, G. Ten Brinke, Polymer 49 (2008) 2669–2677.
[42] Y. Liu, M. Li, R. Bansil, M. Steinhart, Macromolecules 40 (2007) 9482–9490.
[43] A.F. Thünemann, S. General, Langmuir 16 (2000) 9634–9638.
[44] D. Tsiourvas, M. Arkas, Polymer 54 (2013) 1114–1122.
[45] D. Marsh, Chem. Phys. Lipids 165 (2012) 59–76.
[46] D.M. Small, J. Lipid Res. 25 (1984) 1490–1500.
[47] A.F. Thuenemann, Langmuir 16 (2000) 9634–9638.
[48] M.C. Luyten, G.O.R. Alberda van Ekestein, G. Ten Brinke, J. Roukolainen, O. Ikkala, M. Torkkeli, R. Serimaa, Macromolecules 32 (1999) 4404–4410.
[49] E.A. Ponomarenko, A.J. Waddon, D.A. Tirrell, W.J. MacKnight, Langmuir 12 (1996) 2169–2172.
[50] J.L. Lee, E.M. Pearce, T.K. Kwei, Macromolecules 30 (1997) 6877–6883.
[51] N. Canilho, M. Scholl, H.A. Klok, H. Mi, R. Mezzenga, Macromolecules 40 (23) (2007) 8374–8383.
[52] D. Chapman, J. Chem. Soc. 1957 (1957) 4489–4491.
[53] B. Ren, Z. Cheng, Z. Tong, X. Liu, C. Wang, F. Zeng, Macromolecules 39 (2006) 6552–6557.
[54] G.G. Roberts, Langmuir Blodgett Films, Plenum Press, New York, 1990.
[55] W.Y. Gao, Z.W. Yu, Chin. J. Chem. 26 (9) (2008) 1596–1600.
[56] M. Tolan, X-ray Scattering from Soft Matter Thin Films, Springer, Berlin, 1999.
[57] F. Lehmkuhler, M. Paulus, S. Streit-Nierobisch, M. Tolan, Fluid Phase Equilib. 268 (2008) 95–99.
[58] A. Nelson, J. Appl. Crystallogr. 39 (2006) 273–276.
[59] A. Gibaud, S. Hazra, Curr. Sci. 78 (2000) 1467–1477.